batteries

MDPI

Article

A Novel Efficient Grading of Spent Lithium-Ion Batteries Using Electrochemical Impedance Spectrometry

Ote Amuta * and Julia Kowal *

Department of Electrical Energy Storage Technology (EET), Institute of Energy and Automation, Technische Universität Berlin, Einsteinufer 11, 10587 Berlin, Germany
* Correspondence: ote.amuta@campus.tu-berlin.de (O.A.); julia.kowal@tu-berlin.de (J.K.)

Abstract

With the increasing adoption of lithium-ion batteries (LIBs) as the batteries of choice in electromobility, personal electronic devices, and so on, comes the challenge of ageing, which prevents the batteries from performing optimally and meeting the design intent. This is observed in the form of declining power capability due to the increase in resistance and the reduction in capacity that can be stored or discharged from them. Unfortunately, the cost of assessing batteries after the first use remains a daunting challenge. In our work, we propose an approach that carries out fast preliminary grading based on resistance and capacity by first connecting old cells of the same chemistry and model in series with resistors to limit the branch current, then connecting the branches in parallel to equalise the voltages. A Simulink model of NCR18650PF Panasonic cells with adaptive-series resistance is compared with a fixed-series resistance and found to improve the balancing time from over 24 h to just 8 h. Electrochemical impedance spectroscopy (EIS) was carried out on the individual balanced cells between 0.1 Hz and 5 kHz so that the real impedance, imaginary impedance, absolute impedance, and phase were compared with the SOH of the cells at each frequency. Results show that the imaginary impedance in the 6.6 Hz frequency range shows a good correlation coefficient > 0.98 with the SOH, especially with a state of charge (SOC) of about 75–85% for the LCO cells. By selecting only a sample from all the cells that covers a wide range of ages and carrying out a full-capacity checkup on them, a simple correlation with the SOH and the EIS measurements for different frequencies can be used to estimate the SOH of the other cells that were connected in the same parallel connection. This is a considerable time saving in the charge and discharge time on the other cells in facilities that lack the capacity for simultaneous cycling of all cells. There are also huge energy savings in not having to cycle all the cells. Therefore, it offers a more efficient approach to grading spent cells than carrying out full capacity tests.

Keywords: lithium-ion battery; grading; second life

Academic Editor: Cengiz Ozkan

Received: 25 September 2025
Revised: 24 October 2025
Accepted: 29 October 2025
Published: 3 November 2025

Citation: Amuta, O.; Kowal, J. A Novel Efficient Grading of Spent Lithium-Ion Batteries Using Electrochemical Impedance Spectrometry. *Batteries* **2025**, *11*, 404. https://doi.org/10.3390/batteries11110404

1. Introduction

With the increasing adoption of lithium-ion batteries (LIBs) as the batteries of choice in electromobility, personal electronic devices, and so on, comes the challenge of ageing, which prevents the batteries from performing optimally and meeting the design intent. This is observed in the form of declining power capability due to the increase in resistance and the reduction in capacity that can be stored or discharged from them. Many aged batteries used in high-power and high-capacity applications, such as in electric cars, which are no longer fit for purpose, have been deployed in other stationary energy systems, with a

second life [1]. This has increased the amount of research into the second-life possibilities of lithium-ion batteries. Unfortunately, the cost of assessing batteries after the first use remains a daunting challenge. On many occasions, the historical data of batteries during their first life is also unknown, which further compounds the problem [2]. Additionally, with age, battery modules within battery packs begin to vary considerably. At the same time, the individual cells within a module change over time. This implies that for better assessment of the possibility of a second life, it is advisable to separate battery modules into individual cells because there is a chance that only a few cells within a module or modules within a pack may be contributing significantly to the overall ageing of the battery pack [3].

Therefore, to repurpose batteries for a second life, a quick assessment of many cells' remaining capacity and internal resistance becomes expedient. This information will enable operators to grade their cells based on the performance matrix so that cells of similar ageing states are combined in new applications. This performance assessment significantly impacts person hours and cost, despite the other expenses associated with repurposing batteries for second life, such as transportation and dismantling of the battery pack [4]. Several fast grading methods have been proposed. A coulometric counter was used during partial charge between voltage limits to achieve faster capacity estimation of spent battery modules from electric cars compared to the incremental capacity analysis or the constant-voltage charge at maximum voltage [5]. The integral of a cell's voltage during constant-current charge was also used in estimating the SOH of 18650 spent cells obtained from laptops and unknown sources, with good correlation, providing faster cell classification instead of a full capacity check [6]. However, these methods would take a long time if applied to many cells whose capacity may not even be viable for a second life. A quicker checkup can pre-select and grade viable cells before a further substantive test.

Electrochemical impedance spectrometry has also been applied in state-of-health estimation [7], and a detailed explanation of EIS was provided by Lazanas and Prodromidis [8]. Advances in EIS have enabled multisine EIS, in which many sinusoids of different frequencies are coupled to excite the cell [9]. This reduces the time taken to run EIS measurements to a few seconds, making EIS a viable option for fast grading. Unfortunately, the dependence of EIS results on the cell voltage, state of charge, and temperature affects the viability of simply applying it to spent cells with limited knowledge of the state of charge at the beginning of testing.

A notable work was reported in which cells were connected in parallel to balance their voltage; thereafter, they were connected in series and partially charged using a constant current [10]. In the work, the internal resistance was obtained, and the voltage and capacity profile during the partial charge was used to build a neural network model and a linear fit model to achieve fast capacity estimation of all the cells that were connected in parallel. A capacity check-up was then carried out on a few cells among those that were connected in parallel. These few cells became the reference for grading the remaining cells based on the partial discharge profile. The promise in the speed of this assessment method is based on connecting as many cells in parallel as possible. Similar work applied partial discharge at the same C-rate to classify spent cells based on the resistance and capacity [11]. Each spent cell was individually charged to a set voltage, and the open-circuit voltage after relaxation was used to grade them based on internal resistance. It was followed by a discharge with the cells connected in series, with the voltage profile after the instantaneous drop due to resistance related to the cell's capacity. Accurate classification was achieved by training a radial basis function neural network (RBFNN) with the result. Ref. [12] used the genetic algorithm and a backpropagation (GA-BP) model on similar data and achieved capacity estimation with a maximum error of 2.951%. The downside of the approaches outlined above is the complexity of the switching circuit between parallel and

series connections of the cells. Apart from the time taken during the parallel connection to bring the terminal voltages to the same values, the partial charge took 5 min, not to mention the further analysis.

In our work, we propose an approach similar to that proposed in [10] that also connects spent cells of an exact model with a unknown state of health in parallel for voltage equalisation, but electrochemical impedance spectroscopy (EIS) measurement is used instead of partial charging for fast preliminary grading as an early step in the performance-based assessment of spent lithium-ion cells before they can be used for second-life applications. This grading stage comes after physical checks, where cells with visible swelling or corrosion are discarded for recycling. A full capacity check is carried out on a sample among the cells that were connected in parallel, and the correlation between the state of health (SOH) of the cell and the EIS measurement is used to estimate the SOH of the remaining cells.

In the following, Section 2 discusses the effect of the parallel connection on the cells and the method adopted to carry out this work. The results and discussion are presented in Section 3, and the conclusion is reported in Section 4.

2. Methodology

2.1. Cell Balancing with Fixed Resistance

In order to meet voltage and power requirements, many cells are connected in series. It is important that the state of charge (SOC) of the cells, which is the ratio of the current capacity that is available for use to the available capacity, be similar. This is so that the cell with the lowest SOC among the pack does not limit the discharge capacity [13]. During charging, cells with higher SOC values can limit the amount of capacity that can be stored. This is the reason for cell balancing in cells or modules in series while the battery is in service. Passive balancing uses resistors to discharge cells with capacity, considering the voltage difference between individual cells. Active balancing involves discharging cells with a higher SOC cells with a lower SOC, thereby equalising their SOC values. In this work, there is no requirement for higher voltage, as we connect all the spent cells of similar models and ratings in parallel. During operation, parallel-connected cell balancing is deemed unnecessary because the cells automatically balance each other by voltage difference and there is no significant improvement in capacity with or without balancing. The apparent advantage of balancing in parallel connections is that overcurrents can be reduced in cells so that they degrade almost equally [14].

In our work, however, we do not intend to connect the cells to a load but to balance the cells so that their EIS data can be compared and analysed. Directly connecting cells with SOC values and ageing states in parallel comes with serious risks. For example, due to the lower internal resistance of batteries, a small voltage difference of just 0.1 V between cells in parallel results in a high inrush current in some cells. A significantly high current may flow through cells of lower impedance, leading to high heat generation and thermal runaway [15]. Another factor to consider is that the resistances of the spent cells, even if they had the same operating conditions in their first life, are so varied that the current distribution between the cells in parallel can lead to extreme currents in certain cells [16]. The current distribution in each branch is influenced by the relative temperature between cells, the individual open-circuit voltage (OCV), and impedance [17]. Since spent cells can have varied voltage levels before testing, a series resistor can be connected to each cell in order to limit the current that flows through the cells, and each branch can be connected in parallel, as shown in Figure 1.

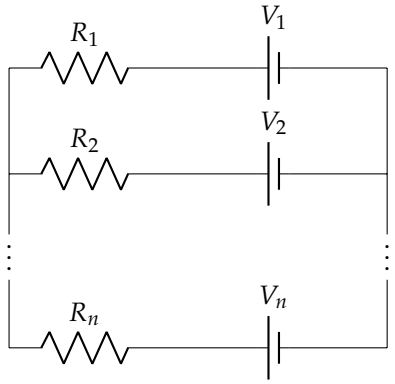

Figure 1. Parallel connection of spent cells.

When connecting the cells in parallel, the voltage (V_p) across the parallel connection is approximately the average of the voltage of the individual cells.

$$V_\mathrm{p} = \frac{1}{n}\sum_{i=1}^{n} V_i \tag{1}$$

Therefore, the instantaneous current that will flow through each cell becomes

$$I_i = \frac{V_\mathrm{p} - V_\mathrm{i}}{R_\mathrm{i}} \tag{2}$$

The value of this current is critical for the safety and performance of the setup because it can cause a temperature rise within the cell; therefore, R_i is selected to ensure that the current is within safe limits. The internal resistance of the cell also affects the current, as a high resistance will lead to lower current flowing through the branch. In a setup of nine cells, assuming that a single cell has a 0% SOC at, say, 3.0 V and the other eight cells have a maximum voltage of 4.2 V, where the cells are connected in series with a 1.5 Ω, the maximum current that will flow through the cell with low SOC is roughly 0.711 A. For spent cells with little information about their health, we propose a current limit of 0.2 C. The current flowing through the cells will slowly decrease because the voltage difference decreases as the cells with a higher SOC discharge and the cells with a lower SOC charge. Thus, using a fixed resistance in series with the cells will take considerable time before the cells achieve the same equilibrium voltage.

2.2. Cell Balancing with Adaptive Resistance

Another approach is to use a variable resistance that adaptively changes based on the voltage difference between the overall parallel connection and individual cell voltages. As a proof of concept, an inbuilt battery model for 18650 cells in MATLAB R2024a Simulink, as shown in Table 1, was used to examine the improvement in time when using adaptive variable resistance.

Table 1. Simscape NCR18650PF battery model.

Specification	Description
Part number	NCR18650PF
Manufacturer	Panasonic
Capacity	2.84 Ah
Voltage	2.5–4.2 V

The Simulink model is shown in Figure A1. The lookup table is shown as a plot in Figure 2 below, in which the series resistance is adaptively changed based on the difference between the average parallel voltage and the individual cell voltage. These values were iteratively selected to ensure that the series current as measured in the simulation is just about 0.5 A. Three different scenarios are tested below.

- Case 1: Eight cells at 100% SOC (4.2 V) and one cell at 0% SOC (3.0 V) with fixed resistance of 2.4 Ω.
- Case 2: Same configuration as Case 1, with adaptive resistance as shown in Figure 2.
- Case 3: Each of the nine cells has SOC values of 20%, 30%, . . . , 100%, with adaptive resistance as shown in Figure 2.

The results of the different cases above are shown in Figure 3, which shows that the cell voltages converge to their average while the current flowing through each branch slowly converges to zero. The time it takes for the cell voltage to converge is over a day for the fixed resistor because as the voltage level equalises, the current flowing through each cell also reduces significantly so that less charge or discharge takes place with the passage of time. With adaptive resistance, once the voltage drops to a new threshold, the resistance is also reduced in order to raise the current that flows within the safe limit by shortening the balancing time to 8 h. Designing the adaptive circuit is beyond the scope of this work; however, the time improvement from this simulation result will be used in comparing the performance of this procedure with that of other methods. In this work, a fixed resistor of 1.5 Ω was connected in series with the cell before connecting the branches in parallel to balance the voltages of the cells, and when the difference between the maximum and minimum voltage dropped to 0.02 V, the cells were connected in parallel. This was done to reduce the time required for the voltage to reach equilibrium.

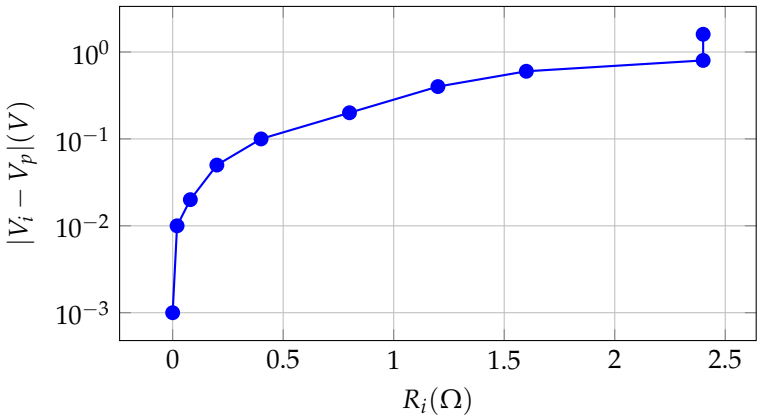

Figure 2. Step plot of resistance vs. voltage difference.

2.3. Test Procedure

The cells in Table 2 were obtained mostly from old laptop battery packs and other unknown sources. The cell labels indicate that the individual cells were taken from similar first-life applications. Three cells (L123–L125), and six of the Panasonic cells (L141–L146) were combined into set 1, comprising nine cells that were connected to the balancing circuit at the same time. Set 2 consists of three sets of three cells (L126–L128, L141–L143, and L431–L433), together making nine cells. The nine cells (L431–L439) were also combined to form set 3. Similarly, set 4 is made up of D71–D73 and T21–T26, while set 5 consist of C92–C95 and H81–H86. The following test was carried out on all nine cells as a set. Further discussion and analysis are also based on each set.

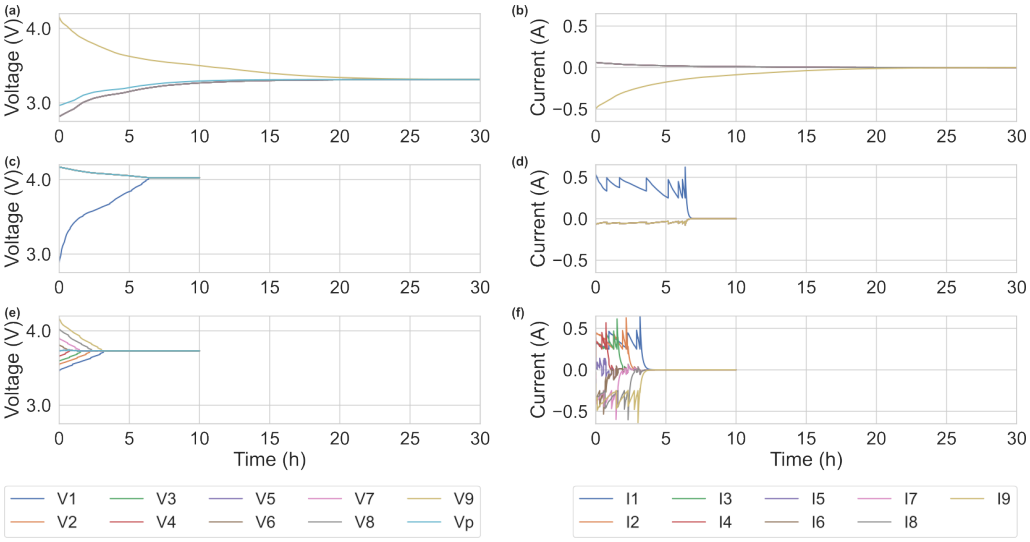

Figure 3. (**a**) Case 1, cell voltages; (**b**) case 1, current flowing through each branch; (**c**) case 2, cell voltages; (**d**) case 2, current flowing through each branch; (**e**) case 3, cell voltages; (**f**) case 3, current flowing through each branch.

Table 2. Test Cells.

Cell Labels	Cell Chemistry	Capacity (mAh)	Model Number	Manufacturer	Comment
L123–L128	LCO/Graphite	2550	CGR18650E	Panasonic	Unknown history
L141–L146	LCO/Graphite	2550	CGR18650E	Panasonic	Old laptop
L431–L439	LCO/Graphite	2550	CGR18650E	Panasonic	Unknown history
D71–D73 T21–T26	NMC/Graphite	2400	US18650GR G7	Sony	Old laptop
C92–C95 H81–H86	NMC/Graphite	2200	US18650GR G5	Sony	Old laptop

First, the cell voltage was measured. This is the first important step, as it immediately tells whether the cell is over-discharged, in which case it is discarded for recycling. This test also tells whether the series resistance designed in the parallel-circuit connection is sufficient. The voltage across the cell also indicates how long the parallel connection will last, since the open-circuit voltage is a function of the state of charge. A wider variation would imply a longer discharge time for cells with higher charge. The readings are recorded.

Following the above result, the cells are connected in parallel, as shown in the circuit diagram in Figure 1. As a safety precaution, the connection order should start with the cell that has the lowest voltage, and the subsequent connection should be to the cell with the next highest voltage. This is repeated until all nine cells are connected in parallel. The voltage terminals of the individual cells were also connected to an Arbin battery tester to observe the voltage profile while in the parallel connection. In addition, a PT100 temperature sensor was placed on the surface of each cell to measure the temperature variation to observe any temperature anomaly due to any cell failure. The setup was also placed in a Mermert ICP110 climate chamber, which was kept at 25 °C. Since the setup used a fixed resistance, it took over 24 h before the voltage range dropped to within 0.02 V, after which the resistor was removed and the cells were bridged. The duration was different for the various sets because of the impact of the internal resistance of each cell and the original voltage. The voltage of the parallel connection was measured and recorded after the voltage was balanced within 5 mV. Subsequently, a Safion Inspectrum EIS meter was used to carry out EIS on each of the nine cells in the set that were individually connected in parallel. This device has a multisine feature that enables fast measurement between

0.1 Hz and 5000 Hz within 20 s and has been widely used on an industrial scale for quality assurance in battery production, offering great potential for fast grading of spent cells.

Subsequently, the cells were connected to an Arbin LBT21084UC battery tester to obtain the capacity of the cells. This step involved discharging with a 0.2 C-rate up to 3 V to find the capacity after the parallel connection. After a rest time of 30 min, the cells were charged using a constant current at a 0.2 C-rate to 4.2 V, then a constant voltage charge until 0.05 C. After a rest of 30 min, a constant current discharge of 0.2 C was used to discharge the cell up to 3 V. The ratio of the full discharge capacity to the nominal capacity was used to calculate the SOH of the cell, and the ratio of the partial discharge capacity after the parallel connection to the full discharge capacity was used to find the SOC of the equilibrium voltage. To compare the resistance EIS result with the incremental capacity analysis, a galvanostatic intermittent titration technique (GITT) was carried out using a 0.2 C pulse for 2.4 min, followed by a rest time of 6 min. This cycle was repeated until full discharge at 3 V. This test schedule is illustrated in Figure 4.

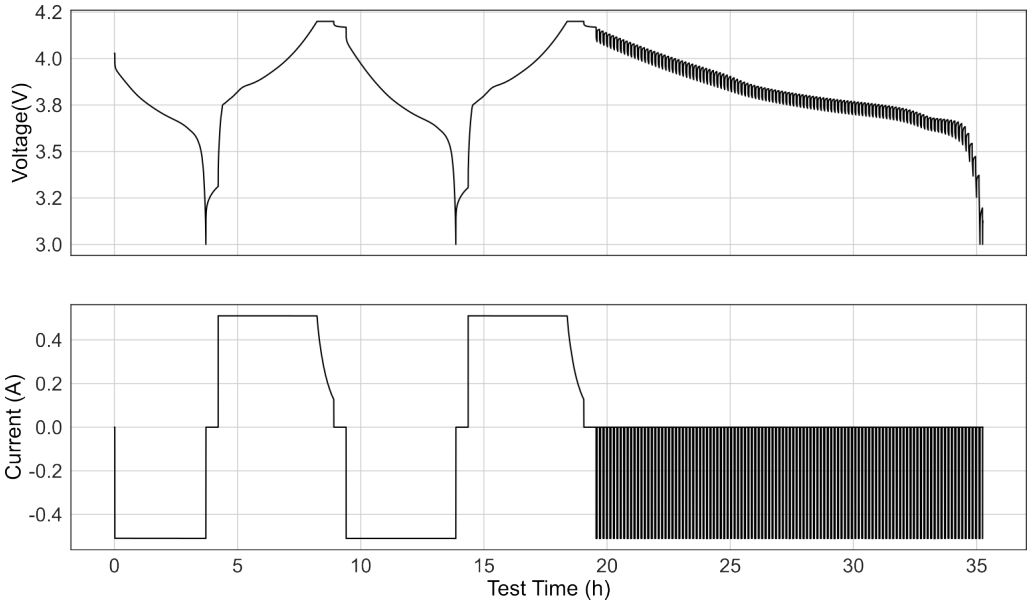

Figure 4. Checkup schedule.

3. Results

3.1. SOH Estimation

Figure 5a shows the voltages before and after the parallel connection for set 1. At the equilibrium voltage, the state of charge is calculated as the ratio of the capacity when discharged to the cut-off voltage (3 V) to the full discharge capacity of the cell. After balancing, the cells had an SOC of about 82%, as shown in Figure 5b. This implies that the parallel connection can get all the cells to have approximately the same SOC after equilibrium. While the cells with higher capacity discharge, the cells with the lower SOC are charged to an equilibrium state. Since the balancing and the EIS measurement were carried out at 25 °C and the SOC is similar for the different cells after balancing, the variation as seen in the negative Nyquist plot (Figure 5c) is indicative of the difference in degradation of the cells at various frequencies, which affects the capacity and the resistance. A shift to the right for the most degraded cell can be observed in the plot.

From the real and imaginary impedance obtained from the EIS measurement, absolute impedance and phase were calculated at each frequency. These values were plotted against the SOH that was obtained from the full capacity discharge at each frequency as shown in Figures A2–A5, which show the relationship between the SOH and the imaginary

impedance, real impedance, absolute impedance, and phase angle, respectively, at the various frequencies of the EIS measurement. The linear correlation analysis was also carried out at each frequency to find the frequency that best fits the SOH, with a mean absolute error (MAE) of 0.4925%. The imaginary impedance shows the best fit at 6.6 Hz, and the expanded view is shown in Figure 5d. This result corroborates the result reported by Chan et al., which posits that the direct impedance measurement from EIS correlates well with the SOH within the low-frequency range [18].

The result of the GITT is shown in Figure 6a, where the direct-current internal resistance (DCIR) is shown at the different SOCs for each cell. The DCIR was obtained from the division of the voltage change by the discharge current while applying a discharge current of 0.2 C as in Equation (3) within the 1 s sample time of the data. The incremental capacity was also obtained by finding the ratio of the discharge capacity (Q) to the change in terminal voltage (V) for each discharge pulse.

$$DCIR = \frac{V_t - V_{t-1}}{I} \tag{3}$$

$$IC = \frac{dQ}{dV} \approx \frac{Q_{pulse-end} - Q_{pulse-start}}{V_{pulse-end} - V_{pulse-start}} \tag{4}$$

The plot shows an apparent variation in the resistance for the respective cells, which indicates the highly degraded cells with the highest resistance. Higher resistance is observed at lower SOC values for cells with minimal ageing behaviour compared to heavily degraded cells. The reverse is the case at higher SOC value. The incremental capacity plot of the different cells is shown in Figure 6b, and the red vertical line signifies the equilibrium voltage of about 4.0275 V after cell balancing. Taking the dQ/dV of this voltage and plotting with the SOH gives Figure 6c, which shows the correlation between the incremental capacity and the SOH at that voltage. With the MAE of 1.5839%, the incremental capacity due to pulse discharge at about that voltage performs less than the correlation of the SOH to the imaginary impedance from the EIS measurement at 6.6 Hz.

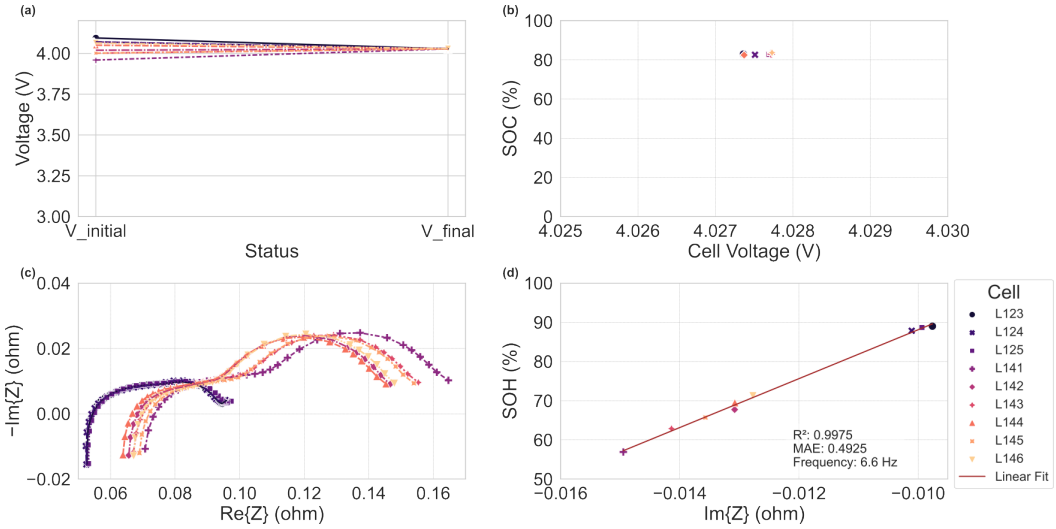

Figure 5. (**a**) Voltage transition in set 1; (**b**) SOC at equilibrium voltage; (**c**) negative Nyquist plot in set 1; (**d**) best-fit imaginary impedance and SOH at 6.6 Hz in set 1.

After balancing the cells of set 2, from their voltage to the equilibrium voltage in Figure 7a, the SOC was about 75%, as shown in Figure 7b. At this SOC, imaginary impedance showed a better correlation coefficient of 0.9848 with the SOH at 0.1 Hz, as shown in Figure 7d. However, the correlation coefficient of 0.9747 at 6.6 Hz can also be

used to estimate the SOH. This indicates that 6.6Hz correlates well with the SOH for this LCO cell and model type. The Nyquist plot in Figure 7c compares similarly to the Figure 6c of set 1. The internal resistance versus SOC, negative incremental capacity versus OCV, and the relationship of the SOH with negative incremental capacity at equilibrium voltage in set 2 are shown in Figure 8a–c. At the equilibrium voltage of 3.9085 V, the incremental capacity plot is somewhat close to the valley for L126–L128. In contrast, the other cells are closer to the peak of the incremental capacity plot. This difference may be responsible for this voltage's lower correlation coefficient of 0.7687.

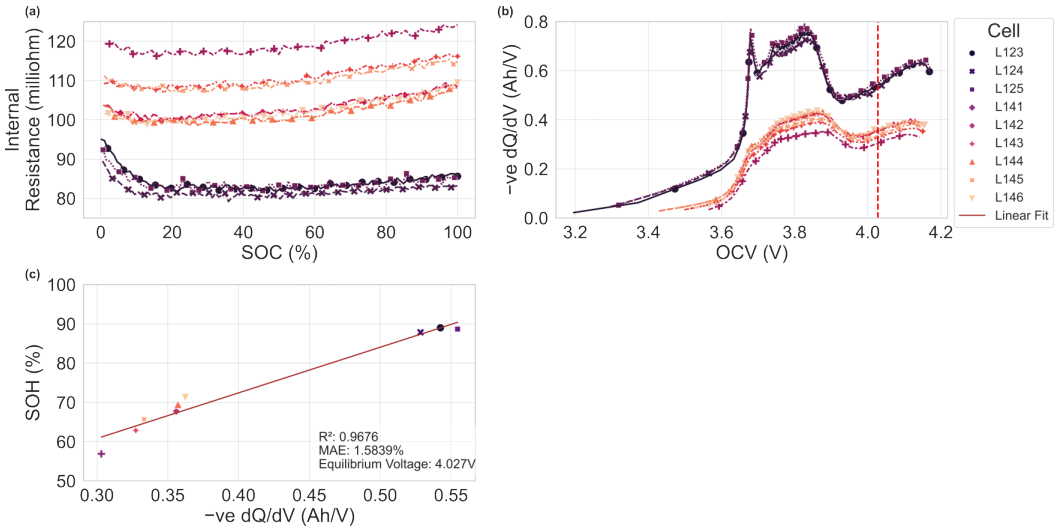

Figure 6. (**a**) Internal resistance vs. SOC; (**b**) negative incremental capacity vs. OCV; (**c**) SOH relationship with negative incremental capacity at equilibrium voltage in set 1.

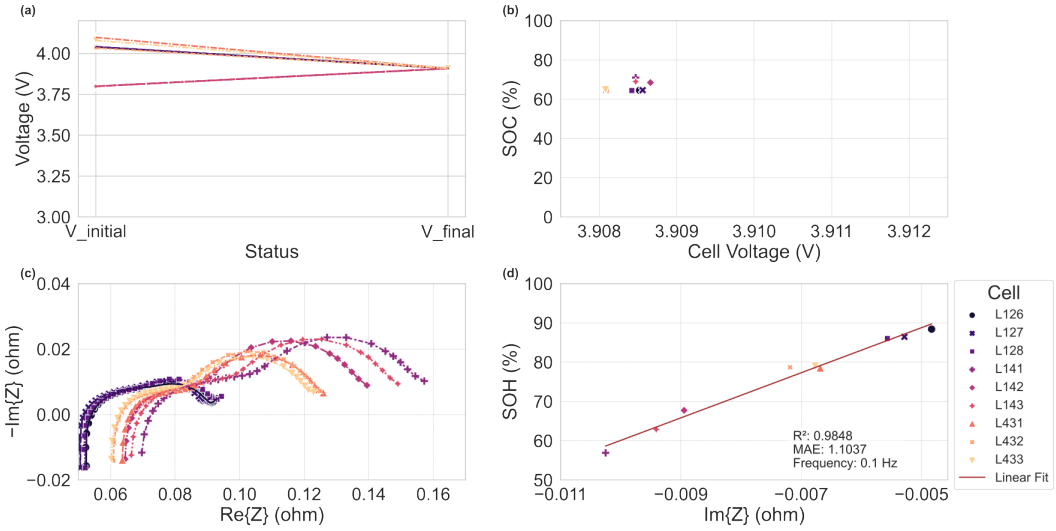

Figure 7. (**a**) Voltage transition; (**b**) SOC at equilibrium voltage; (**c**) Nyquist plot; (**d**) best-fit imaginary impedance and SOH at 0.1 Hz in set 2.

The result for set 3 was different, as shown in Figures 9 and 10, because the SOH values of all nine cells were within the range of 76% to 80%. As a result, there was poor correlation between the SOH and the imaginary impedance, real impedance, and absolute impedance at the different frequencies considered. However, the phase showed a slightly better correlation coefficient of 0.843 at 4.5 Hz. Comparing this to the incremental capacity at the equilibrium voltage of 3.787 V also shows a less distinct feature for each cell, unlike at the voltage above 4.0 V.

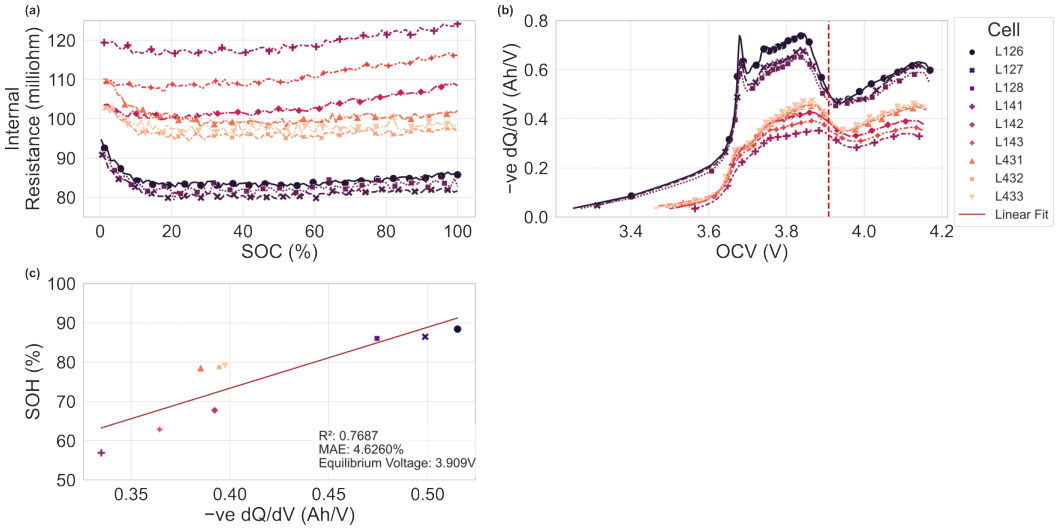

Figure 8. (**a**) Internal resistance vs. SOC; (**b**) negative incremental capacity vs. OCV; (**c**) SOH relationship with negative incremental capacity at equilibrium voltage in set 2.

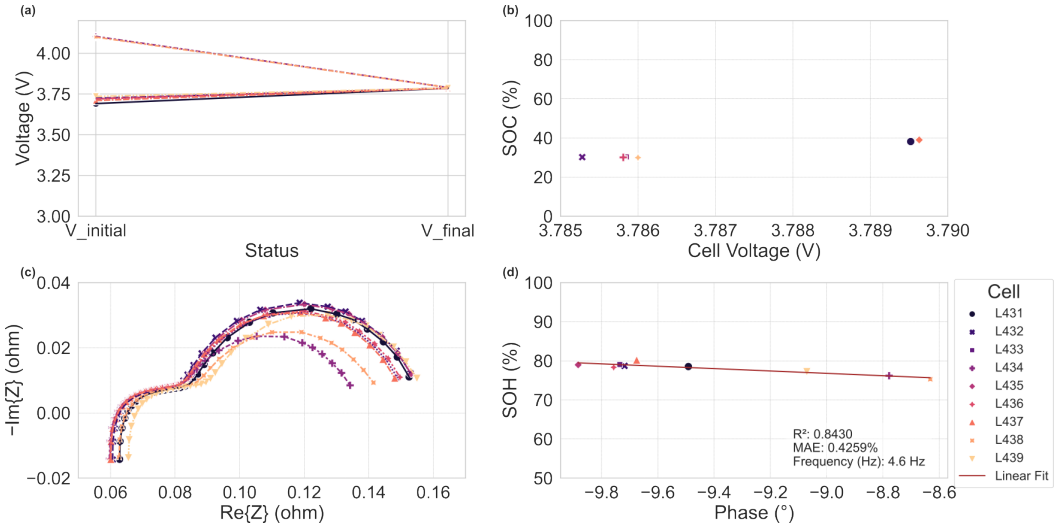

Figure 9. (**a**) Voltage transition; (**b**) SOC at equilibrium voltage; (**c**) Nyquist plot; (**d**) best fit phase and SOH at 4.6 Hz in set 3.

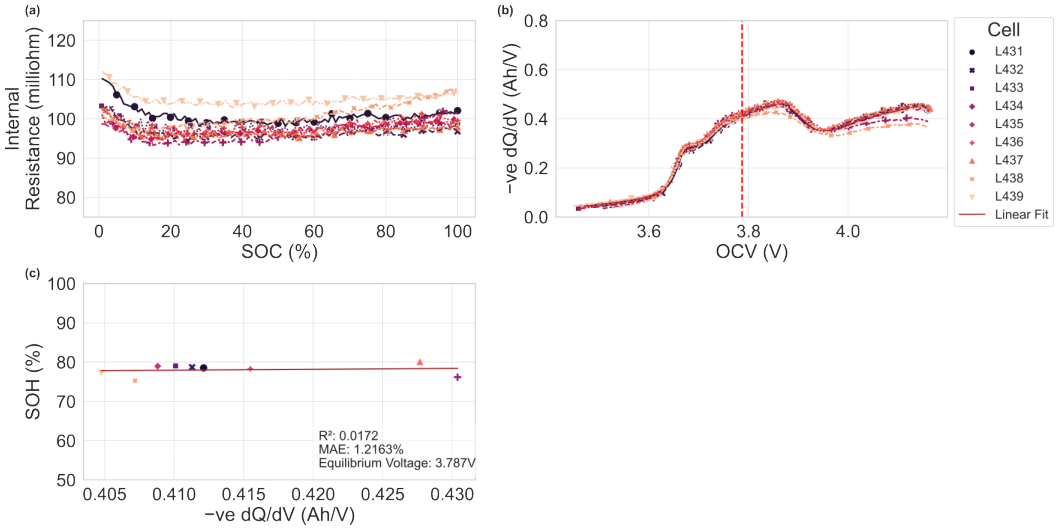

Figure 10. (**a**) Internal resistance vs. SOC; (**b**) negative incremental capacity vs. OCV; (**c**) SOH relationship with negative incremental capacity at equilibrium voltage in set 3.

The SOC of the cells in set 4 after reaching equilibrium voltage was between 46% and 50%, as shown in Figure 11, and a poor correlation coefficient of 0.6977 was observed between the phase angle and the SOH. It appears the small range between their SOH values of 86% to 93% was also responsible for the poor correlation. The correlation between the incremental capacity at the equilibrium voltage and the SOH in Figure 12 was better at 0.8693. This equilibrium voltage is close to the peak of the IC, which corresponds to the equilibrium state in phase transitions of the electrode in the cell [19].

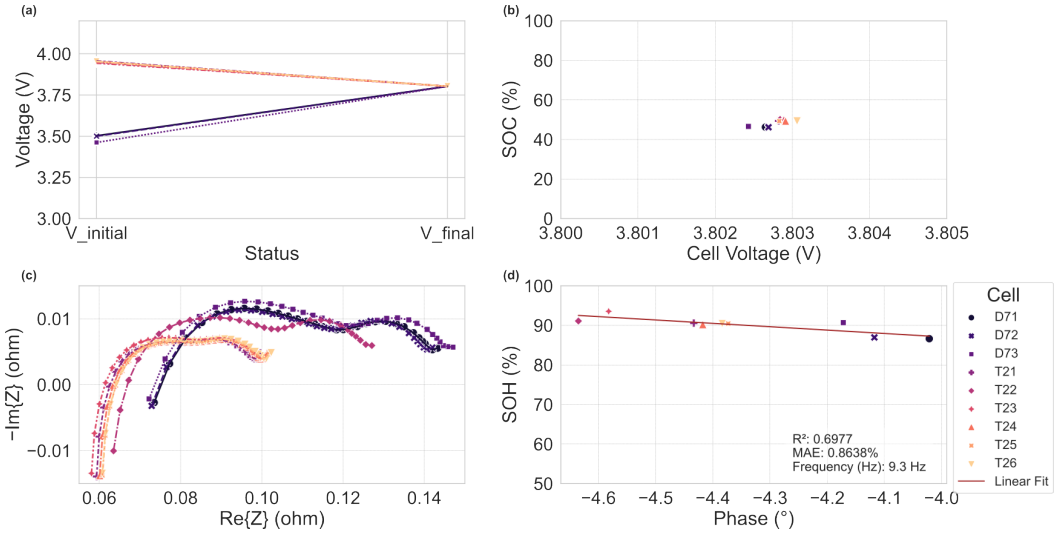

Figure 11. (**a**) Voltage transition; (**b**) SOC at equilibrium voltage; (**c**) Nyquist plot; (**d**) best-fit phase and SOH at 4.6 Hz in set 4.

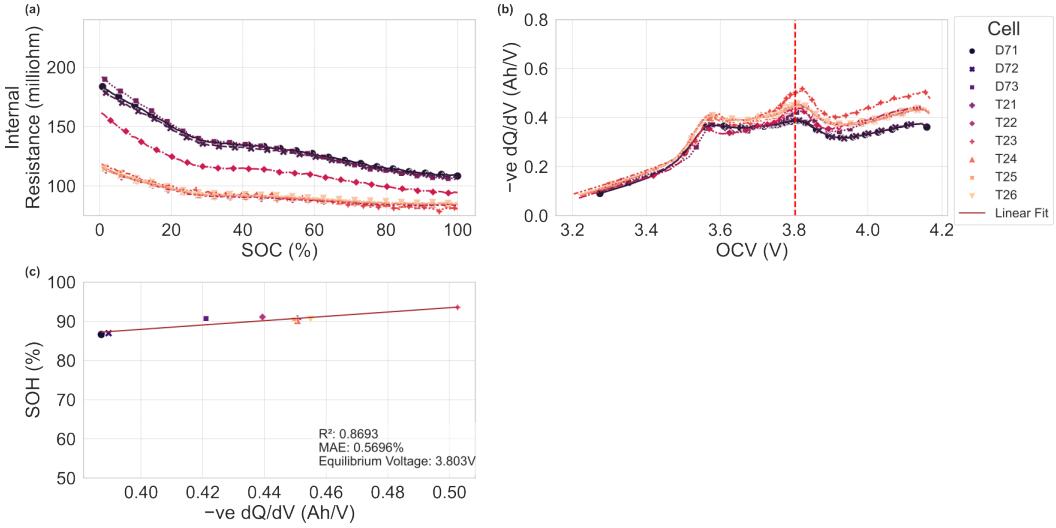

Figure 12. (**a**) Internal resistance vs. SOC; (**b**) negative incremental capacity vs. OCV; (**c**) SOH relationship with negative incremental capacity at equilibrium voltage in set 4.

After the parallel connection in set 5, the equilibrium voltage is about 3.785 V, which corresponds to an SOC of 30% to 42%, as shown in Figure 13. This is a fairly wide variation, and we attribute this to the high impedance of the cells. It can also be observed in the negative Nyquist plot that the EIS for C92, C94, and C95 are somewhat irregular in shape. This can be attributed to the very high impedance, which results in the response of the excitation signal deviating from the linear region of the voltage vs. current density relationship [7]. But for the purpose of comparison with similar cells of different ages, we used the same excitation signals for the EIS measurement for all cells. Despite this high impedance, the imaginary impedance at 9.3 Hz still correlates well with the SOH, with a

coefficient of 0.8933. If we relate this behaviour to the incremental capacity plot in Figure 14, it appears that higher impedance blurs the incremental capacity (IC) plot so much that the peaks are smoothened so that the IC curves for each cell are clearly differentiated from each other, even at low SOC values.

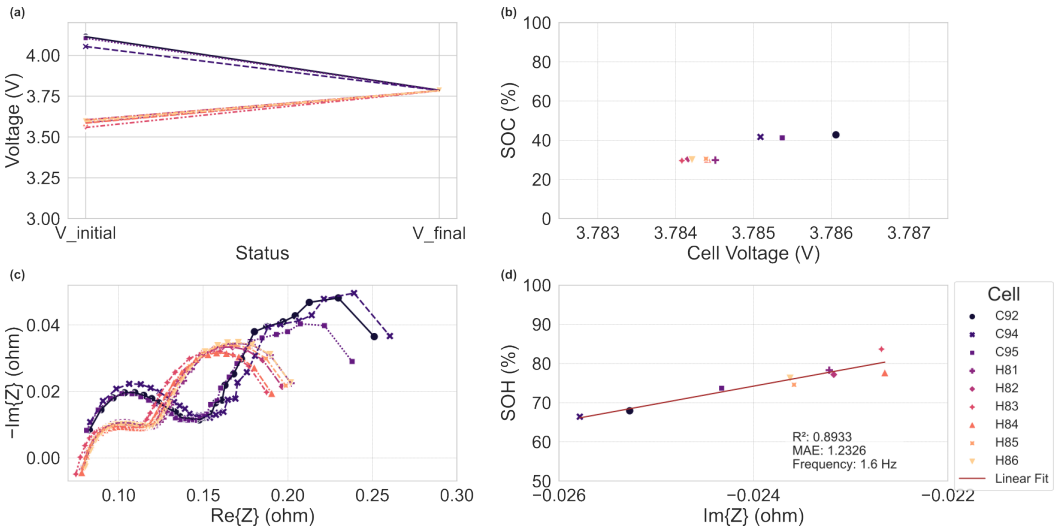

Figure 13. (**a**) Voltage transition; (**b**) SOC at equilibrium voltage; (**c**) Nyquist plot; (**d**) best-fit imaginary impedance and SOH at 1.6 Hz in set5.

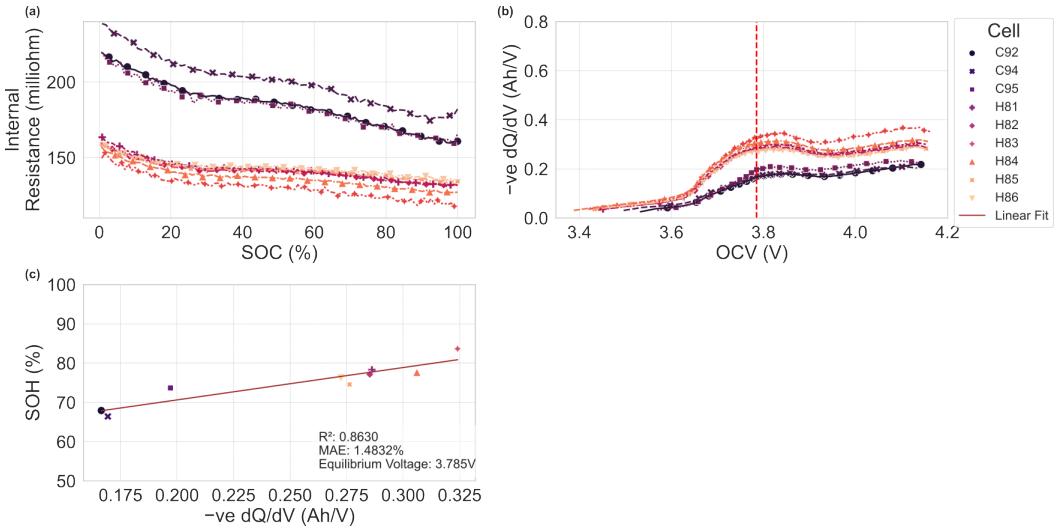

Figure 14. (**a**) Internal resistance vs. SOC; (**b**) negative incremental capacity vs. OCV; (**c**) SOH relationship with negative incremental capacity at equilibrium voltage in set5.

3.2. EIS at Higher SOC

In order to validate the position that the correlation between the imaginary impedance and the SOH is better at higher SOC values, a repeat test was carried out on set 3 and set 4, the SOH ranges of which are only 4% and 7%, respectively. The individual cells were connected to an Arbin battery tester and charged by 1.8 Ah to roughly 80% SOC. The open-circuit voltage was not the same after the charge; thus, the cells in set 3 and set 4 were separately connected in parallel, as presented above, to ensure that the voltages got to the same value. After that, EIS measurement was carried out on each cell, and the correlation analysis was repeated. The result is shown in Figure 15. For set 3 and set 4, the result shows that the imaginary impedance correlates better with the SOH than the phase angles, as per Figures 9d and 11d.

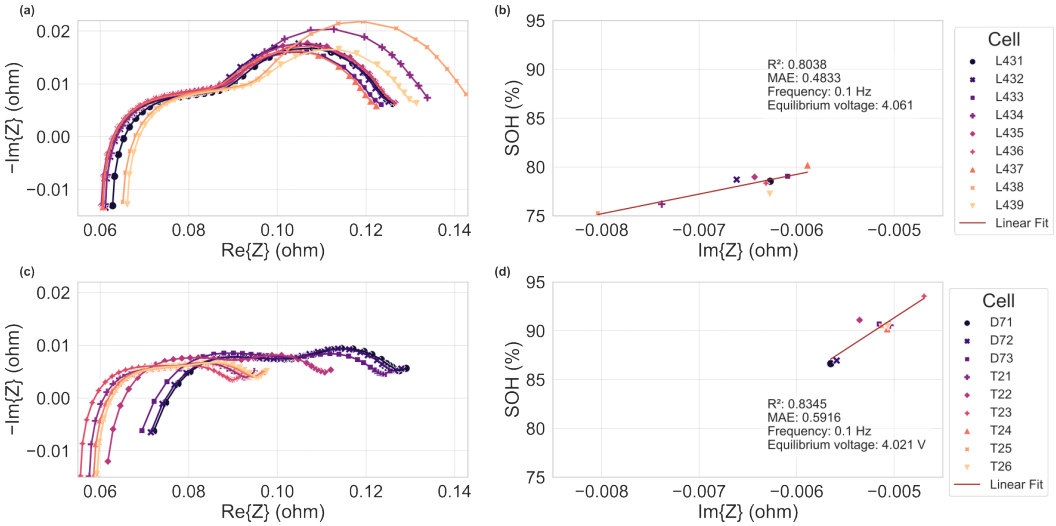

Figure 15. (**a**) Nyquist plot of set 3; (**b**) best-fit imaginary impedance and SOH at 0.1 Hz in set 3; (**c**) Nyquist plot of set 4; (**d**) best-fit imaginary impedance and SOH at 0.1 Hz in set 4.

3.3. Ohmic Resistance

In the Nyquist plot described above, the ohmic resistance refers to the real impedance when the imaginary impedance is zero. If we assume a minimal effect due to the SOC at high frequencies above 1000 Hz, we can group sets 1, 2, and 3 for the LCO cells into one group and plot the ohmic resistance and SOH as in Figure 16a. Similarly, the ohmic resistance and the SOH for set 4 and set 5 are shown as separate groups in the plot. This result proves that the ohmic resistance has a weak correlation with the SOH; however, the overall increase in resistance with decreasing SOH can still be seen in the different sets. From the plot, a grading criterion can easily be identified and selected depending on the possible second-life application requirements. If we assume a requirement for selecting cells that can be grouped into a single application using a clustering diameter of 2.5% SOH, the cells in the shaded circles can be used together in the same second-life application. The other cells, far from each other, can be used separately in other second-life applications. In Figure 16b, it is also observed that the frequency at which the ohmic resistance is obtained increases as the cell ages. This shows that adopting a single frequency, such as 1 kHz, for impedance measurement is insufficient to estimate the cell's ohmic resistance.

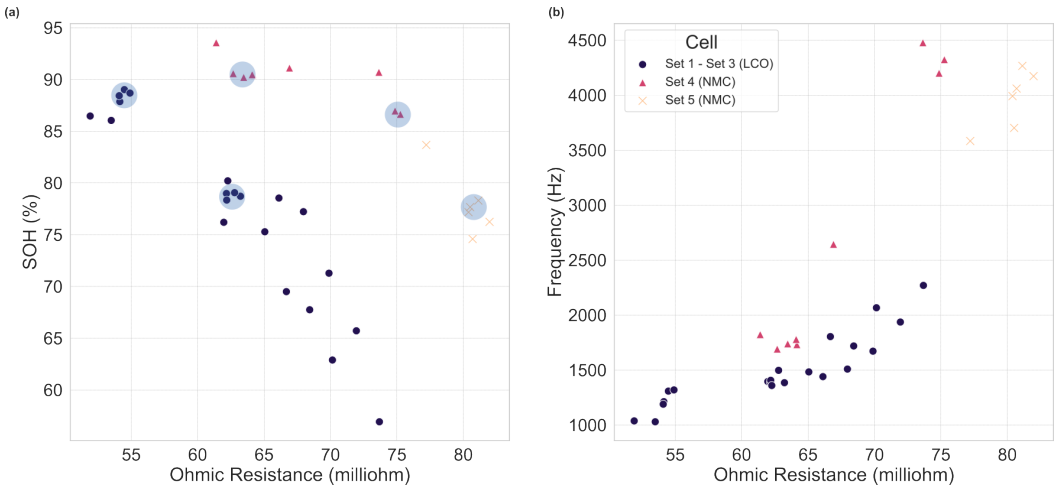

Figure 16. (**a**) Ohmic resistance at zero crossing vs. SOH; (**b**) ohmic resistance vs. frequency.

4. Discussion

It has been established that EIS is affected by the SOC, SOH, and temperature [7]. Temperature effects are not considered in this work because we assume an ambient temperature that can easily be controlled for a second-life assessment facility. Regarding the influence of the SOC on EIS measurement, for example, cells L431–L433, which were included in set 2 and set 3, had different Nyquist plots because their SOC was differed due to the other equilibrium voltage. This explains the reason for analysing only the cells connected in the same parallel connection as a batch so that the influence of the SOC in the assessment can be minimised. Unfortunately, the SOC also influences how the EIS measurement estimates the SOH. This can be observed when comparing the results of set 1 and set 2 of the same cell chemistry and models, where the correlation with the SOH performed better at a higher voltage of 4.0275 V than at a voltage of 3.9085 V. At lower voltages, as in set 3 and set 4, the imaginary impedance did not perform well, but the phase angle has some correlation with the SOH. The IC plots show that the lower-to-medium SOC range is subject to more variation due to the significant ageing modes that affect the IC peaks and valleys differently. This makes this region less effective than the higher SOC region. Another factor to consider is that as the cell ages, the polarisation at the lower SOC becomes higher, and there is a gradual increase in the OCV in the region so that the impedance effect becomes pronounced in EIS measurements in that region, thereby affecting the SOH estimate. Set 5, which happens to be in the low SOC range after reaching equilibrium, behaves slightly differently due to the high impedance, which blurs the IC undulation.

The cells in set 2 are used for the time benefit analysis of the novel approach to grading aged LIBs because the three cells (L126–L128, L141–L143, and L431–L433) were from different sources and connected in parallel. Their relative capacities, as seen in Figure 7d, show that it is possible to complete capacity checks on just one from each category, such as L127, L141, and L432. For these three, the frequency that gives the best correlation of the imaginary impedance with the SOH can be used to find the imaginary impedance of the remaining cells that were connected in parallel. Then, with the linear equation obtained from the three reference cells, the capacities of the remaining cells can be estimated. Assuming that it takes 5 h for the charge and discharge time when using a C-rate of 0.2 C for the capacity checkup and 30 min rest between charge and discharge, it will take less than 16 h to discharge a single cell from the equilibrium SOC to 0% SOC, CCCV charge to full capacity, and CC discharge to 0% SOC again. As discussed in Section 2.2, we can assume 8 h for the cells to balance when connected in an adaptive-series resistance parallel connection. Thus, spending 8 h on the 9 cells and just 16 h on each of the 3 cells for the capacity checkup instead of the nine cells is a time savings of 6 cells $\times$ 16 h = 96 h. Note that each EIS measurement runs for 20 s, so if we add the time of connecting the cell to the probes and disconnecting for all nine cells, it is not up to 10 min. A script can efficiently run on the EIS measuring device's computer to conduct the correlation analysis with the SOH. The time spent on the EIS measurement and data analysis can be considered negligible compared to the charge and discharge time. If we scale up this method to simultaneously connect more cells in parallel, such as 12, 24, 32, 64, and so on, depending on the balancing circuit, more time saving can be achieved as simultaneous charging and discharging becomes limited with an increasing number of cells per parallel connection. Since the capacities of the reference cells are already known, extra savings in time, energy, and other resources can be obtained if the reference cells are reused in subsequent parallel connections. Another advantage of this approach is that the initial EIS measurement after the parallel connection can be used to immediately discard some cells due to their very high internal resistance, such as C92, C94, and C95 in set 5 above, as shown in Figure 13a.

Following the result reported above, the grading method is summarised in Figure 17. We propose that this would be suitable for chemistries with an operating voltage range of 3–4.2 V, such as NMC, NCA, and LCO, which do not have a flat OCV curve. Here, cells with very low OCV are simply discarded, as very low OCV values may signify cells with high self-discharge. Cell with voltage within the operating limits are then grouped into sets depending on the designed number of cells per parallel circuit. Note that the higher the number of parallel connections, the shorter the overall assessment time. An average of the voltages of each set gives an approximate final voltage at equilibrium. If the average voltage is above 3.9 V, we may consider such cells to be in the SOC range and proceed with the EIS measurement. However, due to the poor correlation at a low SOC, as described above, we propose increasing the overall SOC by connecting a constant-voltage power source with a current-limiting function. Once the cell reaches equilibrium voltage, EIS measurement can be performed on all cells in the set. A sample size of at least one-third of the number of cells can be taken from the set to cover the broad ageing spectrum. A capacity checkup is carried out on the sample size using a very low current, such as 0.2 C, in order to reduce the impact of high internal resistance on the temperature build-up of a very aged cell. Finally, correlation analysis can be carried out on the sample between the obtained SOH and the EIS measurement at each frequency, and the best-fit frequency is selected and used to estimate the SOH of the remaining cells.

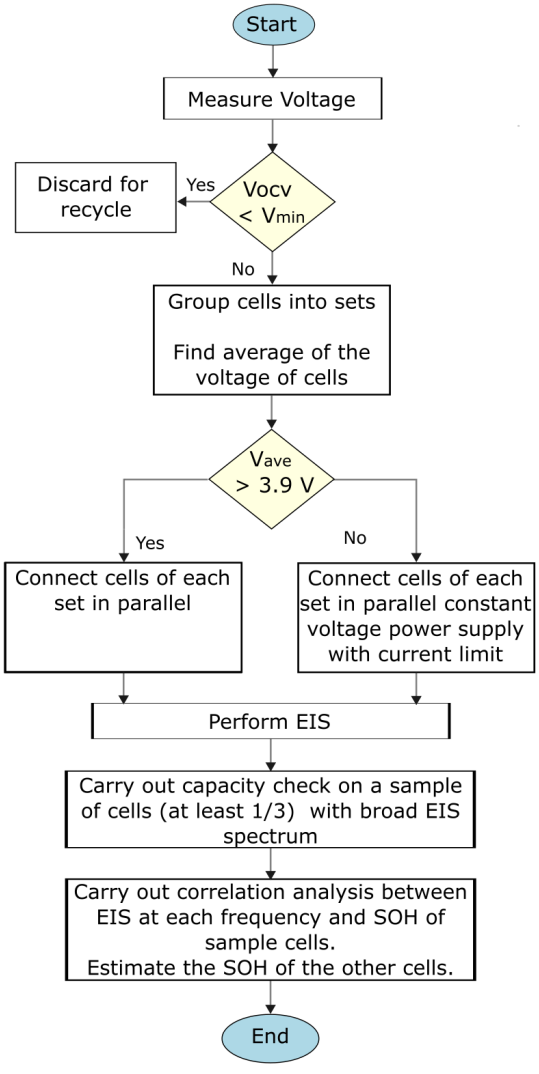

Figure 17. Flowchart for the grading method.

5. Conclusions

Overall, with more degrees of freedom due to phase and imaginary impedance at different frequencies, this method of grading has more possibilities to estimate SOH roughly. The advantage of this grading method is that EIS offers a quick comparison between the group of cells connected initially in parallel, since they already have the same voltage and roughly the same state of charge. This is a considerable time saving in the charge and discharge time on the other cells in facilities that lack the capacity for simultaneous cycling of all cells. There is also huge energy saving in not having to cycle all the cells.

It is essential that when cells are connected in parallel, the final voltage be above their nominal capacity because the lower SOC range may affect the EIS measurement and the corresponding correlation with the SOH. Unfortunately, this depends on the original capacity of the cells before the assessment; an extra charge may be required to raise the SOC of the cells to the preferred range. This experiment was carried out on spent cells with NMC and LCO cathodes, which have OCV values that are nearly proportional to the SOC. For cells with chemistries that have a flat OCV curve, such as LFP cells, this approach should be investigated further to determine its universality.

Cells of the same resistance and capacity have been shown to age differently depending on the cause of the predominant factor leading to their ageing. Hence, further tests, such as the incremental capacity analysis and high-power pulse tests, are needed to further classify the cells based on the similarity of their degradation patternbecause cells with similar internal resistances and capacity do not necessarily age in the same way [20]. Despite these limitations, this approach can help carry out preliminary cell grading. Among the cellsdeemed suitable for a second life, the premium grades can then be subjected to proper incremental analysis, which can be further used for better grouping based on the ageing mechanism.

Future work will involve the design and building of cell-balancing circuitry for a parallel circuit using an adaptive resistance algorithm.

Author Contributions: Conceptualization, O.A.; Formal analysis, O.A.; Investigation, O.A.; Methodology, O.A.; Supervision, J.K.; Validation, O.A.; Visualization, O.A.; Writing—original draft, O.A.; Writing—review and editing, J.K. All authors have read and agreed to the published version of the manuscript.

Funding: This research was funded by the German Academic Exchange Service (DAAD) and the Petroleum Technology Development Fund (PTDF) under the Nigerian–German Postgraduate Training Programme Ph.D., 2022, grant number 57610608.

Data Availability Statement: The dataset is available upon request.

Acknowledgments: We acknowledge support of the German Research Foundation and the Open Access Publication Fund of TU Berlin.

Conflicts of Interest: The authors declare no conflicts of interest.

Abbreviations

The following abbreviations are used in this manuscript:

CCCV	Constant Current, Constant Voltage
DCIR	Direct-Current Internal Resistance
EIS	Electrochemical Impedance Spectrometry
GA-BP	Genetic Algorithm and Back-Propagation

GITT	Galvanostatic Intermittent Titration Technique
IC	Incremental Capacity
LCO	Lithium Cobalt Oxide
LFP	Lithium Iron Phosphate
LIB	Lithium-Ion Battery
MAE	Mean Absolute Error
NCA	Lithium Nickel Cobalt Aluminium Oxide
NMC	Lithium Nickel Manganese Cobalt Oxide
OCV	Open Circuit Voltage
RBFNN	Radial Basis Function Neural Network
SOC	State of Charge
SOH	State of Health

Appendix A

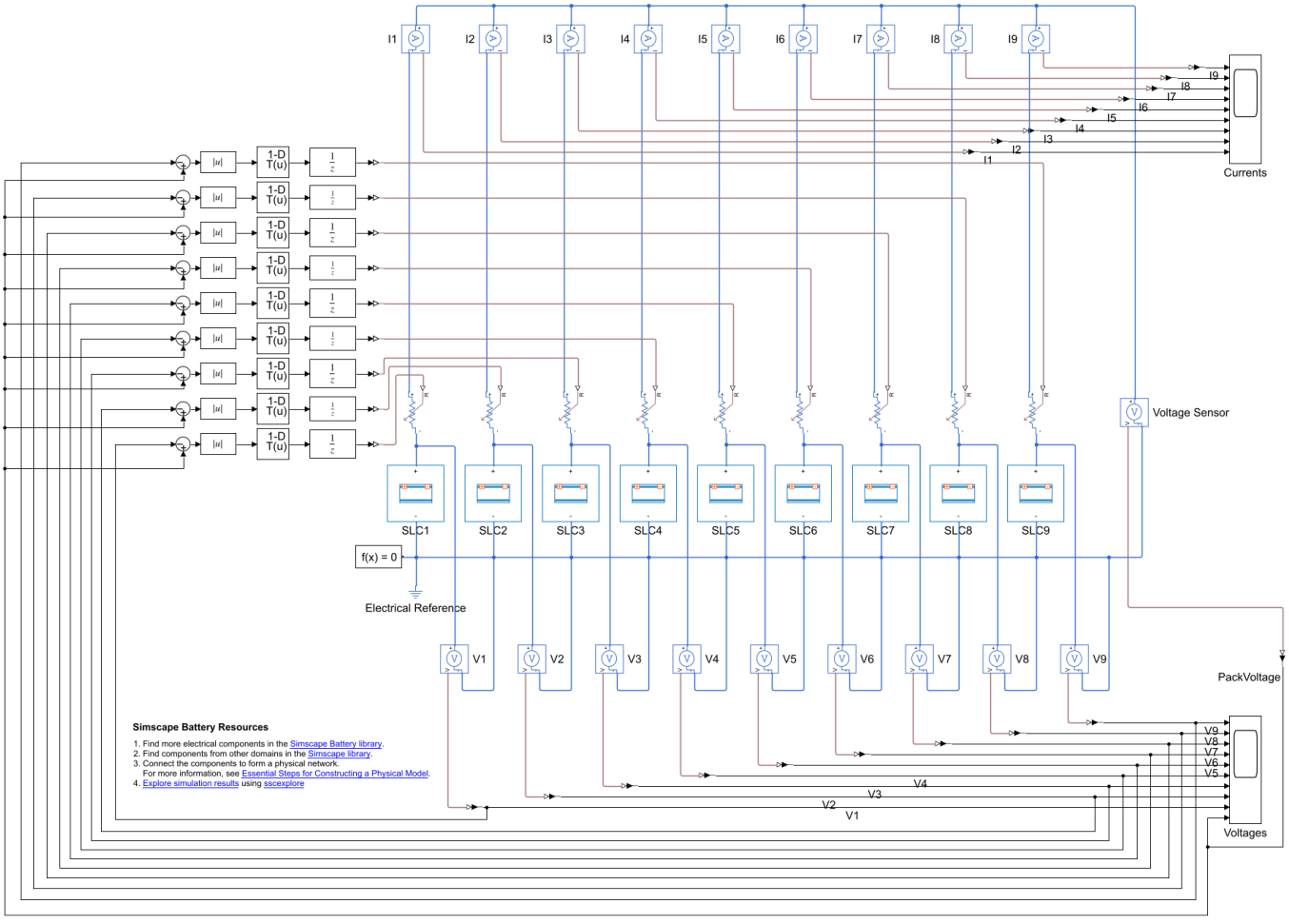

Figure A1. Simulink model.

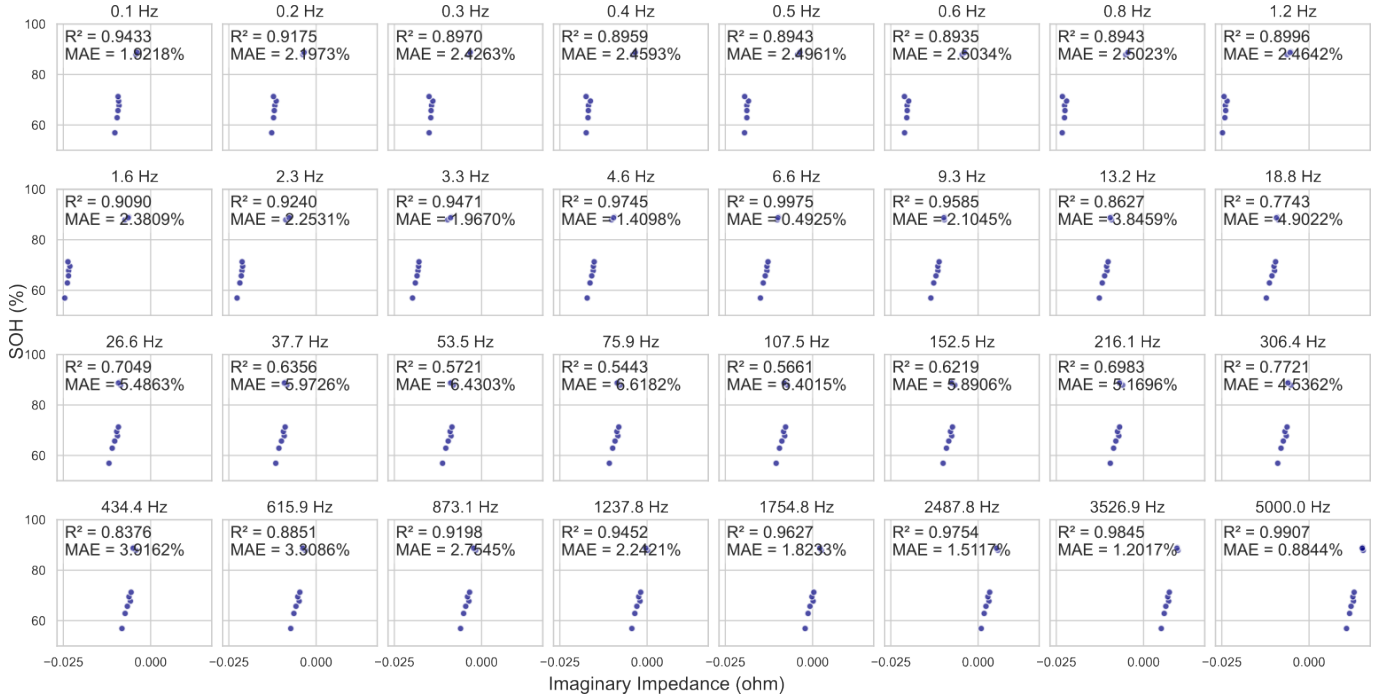

Figure A2. Imaginary impedance vs. SOH in set 1.

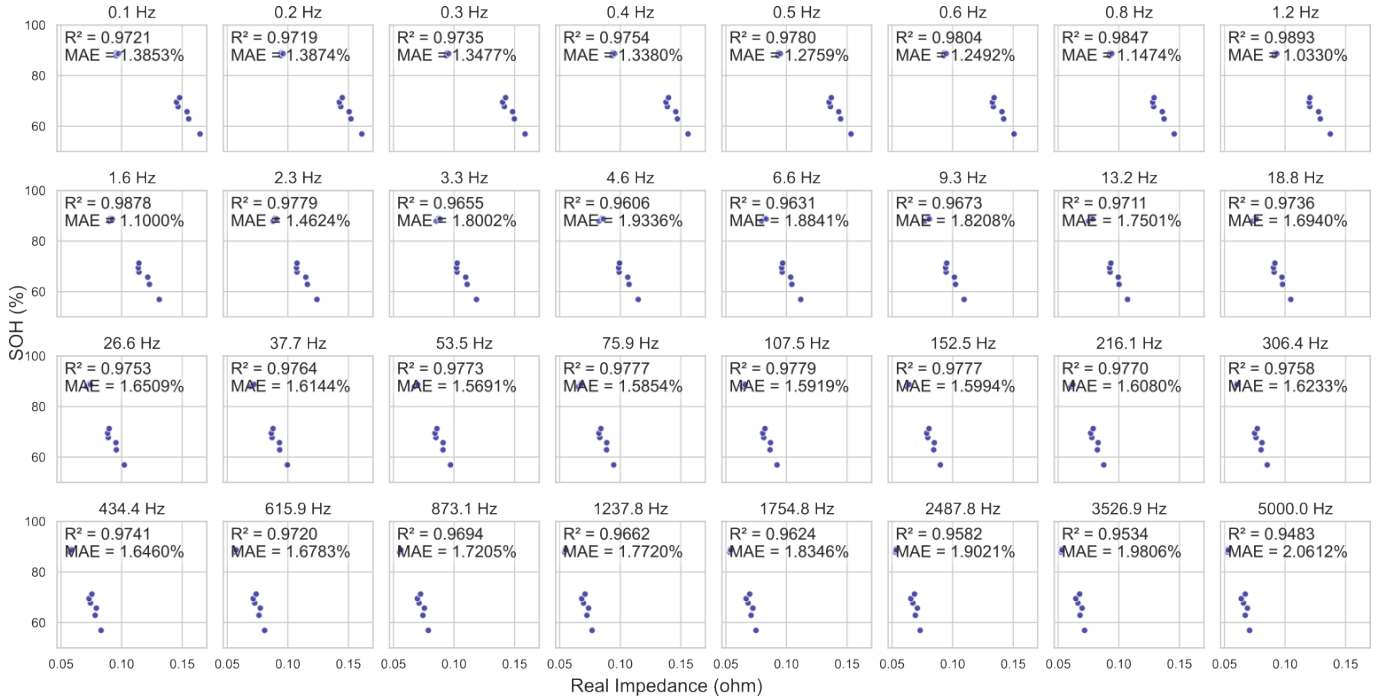

Figure A3. Real impedance vs. SOH in set 1.

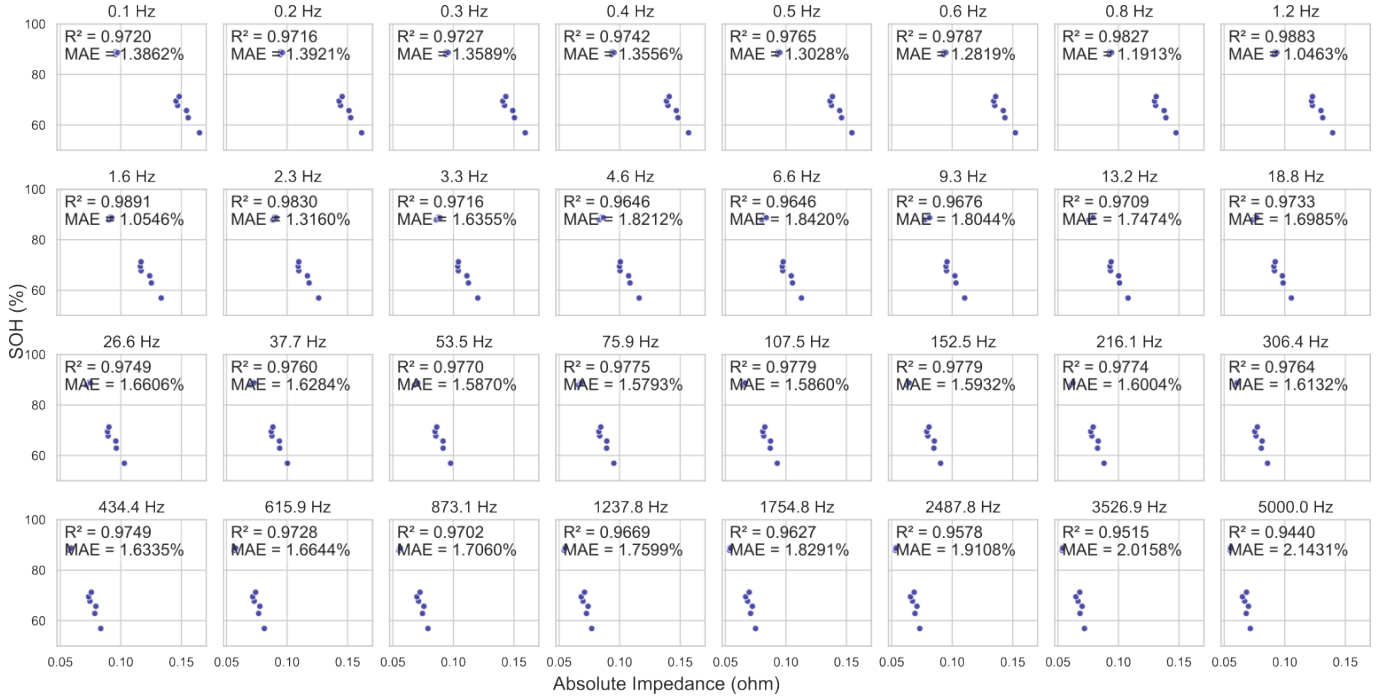

Figure A4. Absolute impedance vs. SOH in set 1.

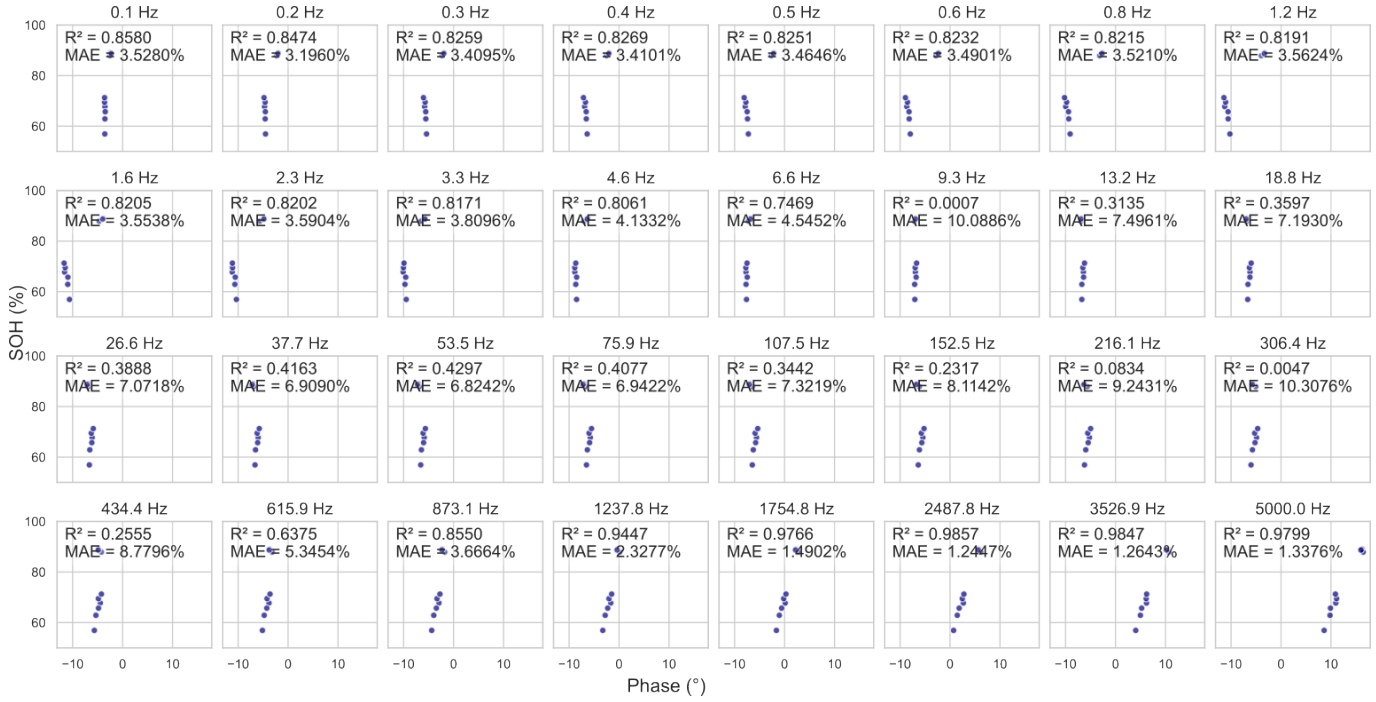

Figure A5. Phase vs. SOH in set 1.

References

1. Faessler, B. Stationary, second use battery energy storage systems and their applications: A research review. *Energies* **2021**, *14*, 2335. [CrossRef]
2. Shahjalal, M.; Roy, P.K.; Shams, T.; Fly, A.; Chowdhury, J.I.; Ahmed, M.R.; Liu, K. A review on second-life of Li-ion batteries: Prospects, challenges, and issues. *Energy* **2022**, *241*, 122881. [CrossRef]
3. Hosseinzadeh, E.; Arias, S.; Krishna, M.; Worwood, D.; Barai, A.; Widanalage, D.; Marco, J. Quantifying cell-to-cell variations of a parallel battery module for different pack configurations. *Appl. Energy* **2021**, *282*, 115859. [CrossRef]
4. Montes, T.; Etxandi-Santolaya, M.; Eichman, J.; Ferreira, V.J.; Trilla, L.; Corchero, C. Procedure for assessing the suitability of battery second life applications after EV first life. *Batteries* **2022**, *8*, 122. [CrossRef]

5. Quinard, H.; Redondo-Iglesias, E.; Pelissier, S.; Venet, P. Fast electrical characterizations of high-energy second life lithium-ion batteries for embedded and stationary applications. *Batteries* **2019**, *5*, 33. [CrossRef]
6. Amuta, O.; Kowal, J. State of Health Assessment of Spent Lithium–Ion Batteries Based on Voltage Integral during the Constant Current Charge. *Batteries* **2023**, *9*, 537. [CrossRef]
7. Meddings, N.; Heinrich, M.; Overney, F.; Lee, J.S.; Ruiz, V.; Napolitano, E.; Seitz, S.; Hinds, G.; Raccichini, R.; Gaberšček, M.; et al. Application of electrochemical impedance spectroscopy to commercial Li-ion cells: A review. *J. Power Sources* **2020**, *480*, 228742. [CrossRef]
8. Lazanas, A.C.; Prodromidis, M.I. Electrochemical impedance spectroscopy—A tutorial. *ACS Meas. Sci. Au* **2023**, *3*, 162–193. [CrossRef] [PubMed]
9. Zappen, H.; Ringbeck, F.; Sauer, D.U. Application of time-resolved multi-sine impedance spectroscopy for lithium-ion battery characterization. *Batteries* **2018**, *4*, 64. [CrossRef]
10. Lai, X.; Qiao, D.; Zheng, Y.; Ouyang, M.; Han, X.; Zhou, L. A rapid screening and regrouping approach based on neural networks for large-scale retired lithium-ion cells in second-use applications. *J. Clean. Prod.* **2019**, *213*, 776–791. [CrossRef]
11. Zhou, P.; He, Z.; Han, T.; Li, X.; Lai, X.; Yan, L.; Lv, T.; Xie, J.; Zheng, Y. A rapid classification method of the retired $LiCo_xNi_yMn_{1-x-y}O_2$ batteries for electric vehicles. *Energy Rep.* **2020**, *6*, 672–683. [CrossRef]
12. Lai, X.; Qiao, D.; Zheng, Y.; Yi, W. A novel screening method based on a partially discharging curve using a genetic algorithm and back-propagation model for the cascade utilization of retired lithium-ion batteries. *Electronics* **2018**, *7*, 399. [CrossRef]
13. Qi, J.; Lu, D.D.C. Review of battery cell balancing techniques. In Proceedings of the 2014 Australasian Universities Power Engineering Conference (AUPEC), Perth, Australia, 28 September–1 October 2014; IEEE: Piscataway, NJ, USA, 2014; pp. 1–6. [CrossRef]
14. Diao, W.; Pecht, M.; Liu, T. Management of imbalances in parallel-connected lithium-ion battery packs. *J. Energy Storage* **2019**, *24*, 100781. [CrossRef]
15. Shimura, J.; Onodera, K.; Watanabe, H.; Shitanda, I.; Itagaki, M. Current Distribution Simulation of Parallel-Connected Modules Using Degraded Lithium-Ion Battery Cells. *EES Batter.* **2025**, *1*, 913–921. [CrossRef]
16. Weng, A.; Movahedi, H.; Wong, C.; Siegel, J.B.; Stefanopoulou, A. Current imbalance in dissimilar parallel-connected batteries and the fate of degradation convergence. *J. Dyn. Syst. Meas. Control* **2024**, *146*, 011106. [CrossRef]
17. Pastor-Fernandez, C.; Bruen, T.; Widanage, W.D.; Gama-Valdez, M.A.; Marco, J. A study of cell-to-cell interactions and degradation in parallel strings: Implications for the battery management system. *J. Power Sources* **2016**, *329*, 574–585. [CrossRef]
18. Chan, H.S.; Dickinson, E.J.; Heins, T.P.; Park, J.; Gaberšček, M.; Lee, Y.Y.; Heinrich, M.; Ruiz, V.; Napolitano, E.; Kauranen, P.; et al. Comparison of methodologies to estimate state-of-health of commercial Li-ion cells from electrochemical frequency response data. *J. Power Sources* **2022**, *542*, 231814. [CrossRef]
19. Barai, A.; Uddin, K.; Dubarry, M.; Somerville, L.; McGordon, A.; Jennings, P.; Bloom, I. A comparison of methodologies for the non-invasive characterisation of commercial Li-ion cells. *Prog. Energy Combust. Sci.* **2019**, *72*, 1–31. [CrossRef]
20. Mowri, S.T.; Barai, A.; Gupta, A.; Marco, J. Modification of degradation mechanism identification technique for cell grading. In Proceedings of the 2021 IEEE Vehicle Power and Propulsion Conference (VPPC), Virtually, 25 October–14 November 2021; IEEE: Piscataway, NJ, USA, 2021; pp. 1–7. [CrossRef]